

See discussions, stats, and author profiles for this publication at: <https://www.researchgate.net/publication/280032863>

The Effect of the Methylation and N-H Acidic Group on the Physicochemical Properties of Imidazolium-Based Ionic Liquids.

ARTICLE in THE JOURNAL OF PHYSICAL CHEMISTRY B · JUNE 2015

Impact Factor: 3.3 · DOI: 10.1021/acs.jpcc.5b05354 · Source: PubMed

READS

67

8 AUTHORS, INCLUDING:



Marisa A. A. Rocha

Universität Bremen

36 PUBLICATIONS 318 CITATIONS

SEE PROFILE



Mara G Freire

University of Aveiro

174 PUBLICATIONS 5,509 CITATIONS

SEE PROFILE



Joao A. P. Coutinho

University of Aveiro

482 PUBLICATIONS 12,279 CITATIONS

SEE PROFILE



Luís M N B F Santos

University of Porto

237 PUBLICATIONS 3,687 CITATIONS

SEE PROFILE

Effect of the Methylation and N–H Acidic Group on the Physicochemical Properties of Imidazolium-Based Ionic Liquids

Ana S. M. C. Rodrigues,[†] Marisa A. A. Rocha,[†] Hugo F. D. Almeida,[‡] Catarina M. S. S. Neves,[‡] José A. Lopes-da-Silva,[§] Mara G. Freire,[‡] João A. P. Coutinho,[‡] and Luís M. N. B. F. Santos^{*,†}

[†]Centro de Investigação em Química, Departamento de Química e Bioquímica, Faculdade de Ciências da Universidade do Porto, R. Campo Alegre 687, P-4169-007 Porto, Portugal

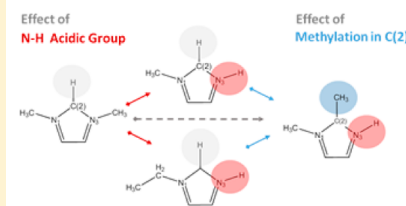
[‡]CICECO - Aveiro Institute of Materials, Chemistry Department, University of Aveiro, Campus de Santiago, 3810-193 Aveiro, Portugal

[§]QOPNA Unit, Departamento de Química, Universidade de Aveiro, 3810-193 Aveiro, Portugal

Supporting Information

ABSTRACT: This work presents and highlights the differentiation of the physicochemical properties of the $[C_1\text{Him}][\text{NTf}_2]$, $[C_2\text{Him}][\text{NTf}_2]$, $[^1C_1^2C_1\text{Him}][\text{NTf}_2]$, and $[^1C_4^2C_1^3C_1\text{im}][\text{NTf}_2]$ that is related with the strong bulk interaction potential, which highlights the differentiation on the physicochemical arising from the presence of the acidic group (N–H) as well as the methylation in position 2, C(2), of the imidazolium ring. Densities, viscosities, refractive indices, and surface tensions in a wide range of temperatures, as well as isobaric heat capacities at 298.15 K, for this IL series are presented and discussed. It was found that the volumetric properties are barely affected by the geometric and structural isomerization, following a quite regular trend. A linear correlation between the glass transition temperature, T_g , and the alkyl chain size was found; however, ILs with the acidic N–H group present a significant higher T_g than the $[^1C_{N-1}^3C_1\text{im}][\text{NTf}_2]$ and $[^1C_N^3C_N\text{im}][\text{NTf}_2]$ series. It was found that the most viscous ILs, ($[^1C_1\text{Him}][\text{NTf}_2]$, $[^1C_2\text{Him}][\text{NTf}_2]$, and $[^1C_1^2C_1\text{Him}][\text{NTf}_2]$) have an acidic N–H group in the imidazolium ring in agreement with the observed increase of energy barrier of flow. The methylation in position 2, C(2), as well as the N–H acidic group in the imidazolium ring contribute to a significant variation in the cation–anion interactions and their dynamics, which is reflected in their charge distribution and polarizability leading to a significant differentiation of the refractive indices, surface tension, and heat capacities. The observed differentiation of the physicochemical properties of the $[^1C_1\text{Him}][\text{NTf}_2]$, $[^1C_2\text{Him}][\text{NTf}_2]$, $[^1C_1^2C_1\text{Him}][\text{NTf}_2]$, and $[^1C_4^2C_1^3C_1\text{im}][\text{NTf}_2]$ are an indication of the stronger bulk interaction potential, which highlights the effect that arises from the presence of the acidic group (N–H) as well as the methylation in position 2 of the imidazolium ring.

PHYSICOCHEMICAL Properties



1. INTRODUCTION

There is increasing interest in ionic liquids (ILs) due to their unusual physical and transport properties which result from their peculiar type of cohesive interactions, charge distribution, and nanostructuration. The molecular structure and supra-molecular organization of an ionic liquid is complex, comprising polar and nonpolar domains. This structural heterogeneity leads to nanostructuration in the bulk which was already observed both theoretically and experimentally.^{1–9} Among their unique properties, the high thermal and chemical stabilities, negligible vapor pressure at room temperature, high ionic conductivity, and improved solvation ability makes them good candidates in a wide variety of applications in the chemical industry, as well as models for the academic understanding of the structural features and interionic interactions in the bulk phase. Most of the studies reported in the literature were focused on the effect of the alkyl chain length and the chemical nature of the ion pairs on the thermophysical properties. There is some work in the literature

that focuses on the effect of the structural isomerism of ionic liquids and how this can affect their thermodynamic properties;^{10–15} however, there is a lack of understanding of the effect of important features like the methylation and N–H acidic bond on physicochemical properties.

The variation in the substituent groups at the cation is found to have a drastic impact in the charge distribution and accessibility.⁸ As a consequence, the anion–cation interaction potential can vary significantly. A case in point is the cation methylation in position 2, C(2), of the imidazolium ring. This structural feature has been investigated by several groups, both experimentally and theoretically, in order to understand its effect on the thermophysical properties and transport properties.^{16–21} This structural modification has been shown to induce a change in the melting temperature, thermal stability, viscosity, surface tension, and heat capacities. The experimental

Received: June 4, 2015

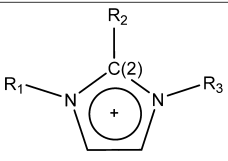
evidence published by Bonhôte et al.¹⁶ showed that the methylation in C(2) of the imidazolium ring of NTf₂-based ionic liquids increases the viscosity by a factor of 2.6, relative to the hydrogenated cation based IL. They also found that the methylation in the C(4) and C(5) positions of the imidazolium has a minor effect.¹⁶ Later on, Hunt¹⁷ used quantum chemical calculations to investigate the effect of the C(2) methylation in the viscosities of imidazolium-based ionic liquids. They found that the increase in the viscosities and melting points is explained by the decrease in melting entropy of the methylated cations, due to a reduction of the number of stable conformers (cation–anion interactions) leading to a decrease of the absolute liquid entropy. Additionally, the free rotation on the butyl chain is restricted by the steric bulk methyl, which limits the position of the anion around the cation. Noack et al.¹⁸ observed the great influence of the C(2) position on the electron density distribution of the molecular structure and on the macroscopic behavior of imidazolium-based ILs, using vibrational and NMR spectroscopy. According to Fumino et al.,^{19,20} the suppression of the hydrogen bonds formed in the C(2) position upon methylation enhances the overall Coulomb interactions between anion and cation. They found that the hydrogen bond formed in C(2)–H disrupted the ionic network by altering the charge symmetry of the ions and thus fluidized imidazolium ILs. These results were supported experimentally by IR spectroscopy where a red-shift and an intensity change of the bands were observed. A theoretical study by Izgorodina et al.²¹ revealed that there is a restriction in the anion movement around the methylated C(2) cation relative to the hydrogenated one with a potential energy barrier exceeding 40 kJ mol^{−1}. Another structural feature that is scarcely addressed in the literature is the acidic hydrogen present in N–H of the imidazolium ring. The ILs comprising this acidic character are more likely to establish hydrogen bonds with the anions and with solvents, such as water.¹⁰

In this work, we explore the structural isomerization effect on the properties of the imidazolium NTf₂-based ILs. Heat capacity, density, viscosity, refractive index, surface tension, and thermal behavior (glass transition, crystallization temperatures/profile, melting temperature, enthalpies and entropies of fusion) are studied here. The change of a group position (such as a methyl group) as well as the presence of the acidic N–H group in the ionic liquid were used as an in situ probe to explore the molecular effects on the overall ionic liquid interaction potential, which will be reflected in their physicochemical properties. Table 1 presents the list and abbreviation of the studied ILs.

2. EXPERIMENTAL SECTION

2.1. Materials and Purification. The 12 IL samples were acquired from IOLITEC with the following state purity: [1C₁Him][NTf₂] (1-methylimidazolium bis-(trifluoromethylsulfonyl)imide, CAS RN: 353239-08-4), >98%; [1C₂Him][NTf₂] (1-ethylimidazolium bis-(trifluoromethylsulfonyl)imide, CAS RN: 353239-10-8), >98%; [1C₁²C₁Him][NTf₂] (1,2-dimethylimidazolium bis-(trifluoromethylsulfonyl)imide, CAS RN: 353239-12-0), 98%; [1C₁³C₁im][NTf₂] (1,3-dimethylimidazolium bis-(trifluoromethylsulfonyl)imide, CAS RN: 174899-81-1), 99%; [1C₂³C₁im][NTf₂] (1-ethyl-3-methylimidazolium bis-(trifluoromethylsulfonyl)imide, CAS RN: 174899-82-2), >99%; [1C₃³C₁im][NTf₂] (1-methyl-3-propylimidazolium bis-(trifluoromethylsulfonyl)imide, CAS RN: 216299-72-8), 99%;

Table 1. Schematic Structures and Abbreviations of the Ionic Liquids under Study

Imidazolium-Based Cations			Abbreviations
			
R ₁ : methyl	R ₂ : hydrogen	R ₃ : hydrogen	[1C ₁ Him][NTf ₂]
R ₁ : ethyl	R ₂ : hydrogen	R ₃ : hydrogen	[1C ₂ Him][NTf ₂]
R ₁ :methyl	R ₂ :methyl	R ₃ :hydrogen	[1C ₁ ² C ₁ Him][NTf ₂]
R ₁ :methyl	R ₂ :hydrogen	R ₃ :methyl	[1C ₁ ³ C ₁ im][NTf ₂]
R ₁ :ethyl	R ₂ :hydrogen	R ₃ :methyl	[1C ₂ ³ C ₁ im][NTf ₂]
R ₁ :propyl	R ₂ :hydrogen	R ₃ :methyl	[1C ₃ ³ C ₁ im][NTf ₂]
R ₁ :ethyl	R ₂ :hydrogen	R ₃ :ethyl	[1C ₂ ³ C ₂ im][NTf ₂]
R ₁ :ethyl	R ₂ :hydrogen	R ₃ :propyl	[1C ₂ ³ C ₃ im][NTf ₂]
R ₁ :butyl	R ₂ :hydrogen	R ₃ :methyl	[1C ₄ ³ C ₁ im][NTf ₂]
R ₁ :pentyl	R ₂ :hydrogen	R ₃ :methyl	[1C ₅ ³ C ₁ im][NTf ₂]
R ₁ :propyl	R ₂ :hydrogen	R ₃ :propyl	[1C ₃ ³ C ₃ im][NTf ₂]
R ₁ :butyl	R ₂ :methyl	R ₃ :methyl	[1C ₄ ² C ₁ ³ C ₁ im][NTf ₂]

[1C₂³C₂im][NTf₂] (1,3-diethylimidazolium bis-(trifluoromethylsulfonyl)imide, CAS RN: 174899-88-8), >99%; [1C₂³C₃im][NTf₂] (1-ethyl-3-propylimidazolium bis-(trifluoromethylsulfonyl)imide, CAS RN: 347882-21-7, >99%; [1C₄³C₁im][NTf₂] (1-butyl-3-methylimidazolium bis-(trifluoromethylsulfonyl)imide, CAS RN: 174899-83-3, >99%; [1C₅³C₁im][NTf₂] (1-methyl-3-pentylimidazolium bis-(trifluoromethylsulfonyl)imide, CAS RN: n.a., >99%; [1C₃³C₃im][NTf₂] (1,3-dipropylimidazolium bis-(trifluoromethylsulfonyl)imide, CAS RN: n.a., >99%; [1C₄²C₁³C₁im][NTf₂] (1-butyl-2,3-dimethylimidazolium bis-(trifluoromethylsulfonyl)imide, CAS RN: 350493-08-2, 99%). The relative atomic masses used in this work were those recommended by the IUPAC Commission in 2007.²²

The commercial IL samples were purified under vacuum (0.1 Pa) at moderate temperature (323 K) and constant stirring for 48 h in order to remove traces of volatile impurities. The water mass fraction content was determined in a 151 Metrohm 831 Karl Fischer coulometer, using a Hydranal-152 Coulomat AG from Riedel-de Haën. The water content, in all ILs, was below 100 ppm. This process was performed systematically, before any experimental measurement.

2.2. Thermal Behavior. Temperatures and the standard molar enthalpies of fusion for the ILs were measured in a power compensation differential scanning calorimeter, PERKIN ELMER model Pyris Diamond DSC, using hermetically sealed aluminum crucibles with a constant flow of nitrogen (50 mL min^{−1}). Samples of about 15 mg were used in each experiment. The temperature and heat flux scales of the power compensation DSC were calibrated by measuring the temperature and the enthalpy of fusion of reference materials,^{23,24} namely, benzoic acid, 4-methoxybenzoic acid, triphenylene, naphthalene, anthracene, 1,3,5-triphenylbenzene, diphenylacetic acid, perylene, *o*-terphenyl, and 9,10-diphenylanthracene, at different scanning rates (2, 5, and 10 K min^{−1}). Each IL sample was previously heated above the melting temperature for 30 min, followed by a quenching step consisting of a fast cooling (~50 K min^{−1}) until 173 K. This procedure avoids the crystallization on cooling and promotes glass formation. After that, the IL samples were heated (5 K min^{−1}) to promote crystallization followed by cooling (~50 K min^{−1}) and heating

Table 2. Experimental Glass, T_g , Cold Crystallization, T_{cc} , Solid–Solid, T_{ss} , Melting, T_m , Temperatures, Enthalpies, $\Delta H(T)$, and Entropies of Transitions, $\Delta S(T)$ for the Studied ILs

ionic liquid	T/K	$\Delta H(T)/\text{kJ mol}^{-1}$	$\Delta S(T)/\text{J K}^{-1} \text{mol}^{-1}$
$[\text{C}_1\text{Him}][\text{NTf}_2]$	321.5 ± 0.5 (T_m)	24.1 ± 0.7	75.0 ± 2.2
$[\text{C}_2\text{Him}][\text{NTf}_2]$	184.2 ± 0.5 (T_g)		
	206.6 ± 0.5 (T_{cc})		
	263.5 ± 0.5 (T_{ss})	1.8 ± 0.7	6.7 ± 2.6
	275.5 ± 0.5 (T_m)	14.2 ± 0.7	51.5 ± 2.5
$[\text{C}_1^2\text{C}_1\text{Him}][\text{NTf}_2]$	311.0 ± 0.5 (T_m)	19.2 ± 0.7	61.7 ± 2.2
$[\text{C}_1^3\text{C}_1\text{im}][\text{NTf}_2]$	176.4 ± 0.5 (T_g)		
	293.2 ± 0.5 (T_m)	22.0 ± 0.7	75.0 ± 2.4
	$[299 (T_m)]^{34}$	$[24.5]^{34}$	$[81.7]^{34}$
$[\text{C}_2^3\text{C}_1\text{im}][\text{NTf}_2]$	178.3 ± 0.5 (T_g)		
	$[186 (T_g)]^{34}$		
	206.8 ± 0.5 (T_{cc})		
	260.0 ± 0.5 (T_m)	21.3 ± 0.7	81.9 ± 2.7
	$[291 (T_m)]^{34}$	$[24.8 \Delta H(T_m)]^{34}$	$[97.1 \Delta S(T_m)]^{34}$
$[\text{C}_3^3\text{C}_1\text{im}][\text{NTf}_2]$	179.6 ± 0.5 (T_g)		
	$[184.0 (T_g)]^6$		
$[\text{C}_4^3\text{C}_1\text{im}][\text{NTf}_2]$	182.1 ± 0.5 (T_g)		
	$[186 (T_g)]^{34}$		
	$[181.5 \pm 0.1 (T_g)]^{36}$		
$[\text{C}_2^3\text{C}_2\text{im}][\text{NTf}_2]$	286.3 ± 0.5 (T_m)	29.1 ± 0.7	101.6 ± 2.4
	$[262.6 \pm 0.1 (T_m)]^{35}$	$[20.4 \pm 0.3]^{35}$	
	$[285.5 (T_m)]^6$		
$[\text{C}_2^3\text{C}_3\text{im}][\text{NTf}_2]$	179.5 ± 0.5 (T_g)		
$[\text{C}_5^3\text{C}_1\text{im}][\text{NTf}_2]$	183.8 ± 0.5 (T_g)		
	$[186.5 (T_g)]^6$		
$[\text{C}_3^3\text{C}_3\text{im}][\text{NTf}_2]$	180.9 ± 0.5 (T_g)		
$[\text{C}_4^2\text{C}_1^3\text{C}_1\text{im}][\text{NTf}_2]$	191.5 ± 0.5 (T_g)		

cycles (5 K min^{-1}) in the crystallization region, exceeding the glass transition and below the temperature of melting to ensure complete crystallization before the melting. A final scan at 5 K min^{-1} was performed to determine the temperatures and enthalpies of the solid–solid and isotropization phase transitions.

2.3. Densities and Viscosities. The density, ρ , and viscosity, η , for the $[\text{C}_1\text{Him}][\text{NTf}_2]$, $[\text{C}_2\text{Him}][\text{NTf}_2]$, $[\text{C}_2^3\text{C}_3\text{im}][\text{NTf}_2]$, and $[\text{C}_1^2\text{C}_1\text{Him}][\text{NTf}_2]$ ILs were measured using an automated SVM 3000 Anton Paar rotational Stabinger viscometer–densimeter. The measurements were carried out at 0.1 MPa in the temperature range from 278.15 to 363.15 K. Only the $[\text{C}_1\text{Him}][\text{NTf}_2]$ and $[\text{C}_1^2\text{C}_1\text{Him}][\text{NTf}_2]$ ILs, which are solids at room temperature, were measured in a narrower temperature range of 323.15–363.15 and 303.15–363.15 K, respectively. For each ionic liquid, at least two independent measurements were performed using the same experimental conditions and different samples. The apparatus was calibrated using the three standard calibration samples, APN7.5, APN26, and APN415 in the same experimental conditions of the ionic liquid measurements. The reproducibility of the viscosity and density measurements is, according to the manufacturer, 0.35% and $\pm 0.5 \text{ kg m}^{-3}$, respectively, from 288.15 to 378.15 K and the uncertainty of temperature is within $\pm 0.02 \text{ K}$. Further details regarding the equipment and method are available in the literature.^{25,26}

2.4. Heat Capacities. The heat capacities at $T = 298.15 \text{ K}$ of the $[\text{C}_1\text{Him}][\text{NTf}_2]$, $[\text{C}_2\text{Him}][\text{NTf}_2]$, $[\text{C}_2^3\text{C}_3\text{im}][\text{NTf}_2]$, and $[\text{C}_1^2\text{C}_1\text{Him}][\text{NTf}_2]$ ILs were measured by a high-precision heat capacity drop calorimeter, described in the literature.^{27–30} The calorimeter was calibrated with water and

sapphire ($\alpha\text{-Al}_2\text{O}_3$).²³ The calibration constant was found to be $\varepsilon = 6.6040 \pm 0.0036 \text{ W}\cdot\text{V}^{-1}$. The accuracy of the apparatus for measurements of heat capacities of liquids and solids was evaluated before, using benzoic acid, hexafluorobenzene, *p*-terphenyl, and $[\text{C}_6^3\text{C}_1\text{im}][\text{NTf}_2]$.²⁹ The ampoules were weighted in a Mettler Toledo AG245 dual range analytical balance (sensitivity of $1 \times 10^{-6} \text{ g}$ and repeatability of $2 \times 10^{-6} \text{ g}$) both empty and after filling with the ionic liquid. All the uncertainties are given as twice the standard deviation of the mean, and include the calibration uncertainty. The buoyancy effect correction was considered for both the calibration and experiments of the ILs.

2.5. Refractive Indices. The refractive indices for all the ILs presented in Table 1 were measured at the sodium D-line using a Bellingham model RFM340 refractometer ($\pm 3 \times 10^{-5}$ stated precision), as a function of temperature. The refractometer features a presser with a seal ring made of fluoropolymer Kalrez which is closed over the sample on the prism preventing/decreasing the IL sample contact with water and atmospheric gases, in particular, CO_2 . The presser incorporates a micro flow cell, which is used to introduce the sample into the refractometer, without opening it to the atmosphere in order to avoid moisture and other gases contamination of the ILs samples. For the studied samples no time drift was detected along the measurements. The presser and the internal prism water jacket assembly is temperature controlled by an external bath through the presser hinge and integral channels in the presser arm. The temperature in the refractometer cell is controlled using an external thermostatic bath within a temperature fluctuation of $\pm 5 \times 10^{-3} \text{ K}$, measured with a resolution better than 1×10^{-3}

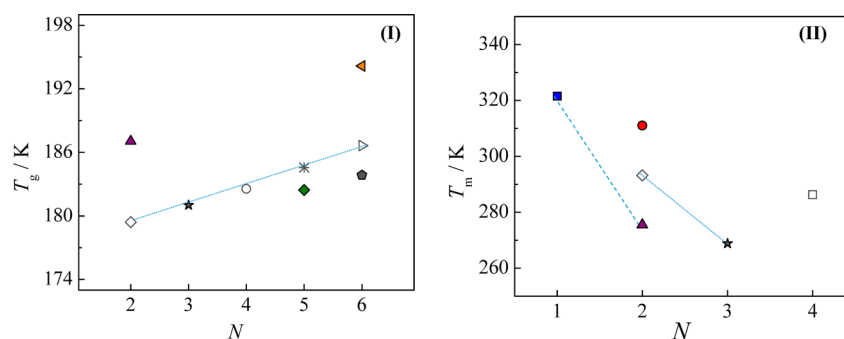


Figure 1. Graphic representation of the glass transitions temperatures, T_g /K, (I), and melting temperatures, T_m /K, (II) as a function of the total number of carbon atoms in the alkyl side chains of the ILs: purple \blacktriangle - $[\text{C}_2\text{Him}][\text{NTf}_2]$; green \blacklozenge - $[\text{C}_2^3\text{C}_3\text{im}][\text{NTf}_2]$; \blacklozenge - $[\text{C}_1^3\text{C}_3\text{im}][\text{NTf}_2]$; \star - $[\text{C}_2^3\text{C}_3\text{im}][\text{NTf}_2]$; \circ - $[\text{C}_3^3\text{C}_3\text{im}][\text{NTf}_2]$; \ast - $[\text{C}_4^3\text{C}_3\text{im}][\text{NTf}_2]$; \triangle - $[\text{C}_5^3\text{C}_3\text{im}][\text{NTf}_2]$; black pentagon - $[\text{C}_3^3\text{C}_3\text{im}][\text{NTf}_2]$; orange \blacktriangle - $[\text{C}_4^2\text{C}_1^3\text{C}_3\text{im}][\text{NTf}_2]$; blue \blacksquare - $[\text{C}_1\text{Him}][\text{NTf}_2]$; red \bullet - $[\text{C}_1^2\text{C}_1\text{Him}][\text{NTf}_2]$; \square - $[\text{C}_2^3\text{C}_3\text{im}][\text{NTf}_2]$. The dashed and dotted lines highlight the $[\text{C}_N\text{Him}][\text{NTf}_2]$ and $[\text{C}_{N-1}^3\text{C}_3\text{im}][\text{NTf}_2]$ series, which have no physical meaning.

K and an uncertainty within ± 0.02 K. The apparatus was calibrated with degassed water (Millipore quality) and toluene (Spectralab, 99.9%). Samples were directly introduced into the flow cell (prism assembly) using a syringe; the flow cell was kept closed after sample injection. For each ionic liquid at least two independent experiments were performed, and in each experiment at least three measurements were taken at each temperature. The refractive indices were measured with respect to air and no corrections were applied.

2.6. Surface Tension. The surface tension of each ionic liquid sample was determined by the analysis of the shape of a pendant drop and measured using a Dataphysics (model OCA-20) contact angle system. Drop volumes of 9 ± 0.5 μL were obtained using a Hamilton DS 500/GT syringe connected to a Teflon coated needle placed inside an aluminum air chamber able to maintain the temperature of interest within ± 0.1 K. The surface tension measurements were performed in the temperature range from 298.15 to 343.15 K, with the exception of $[\text{C}_1\text{Him}][\text{NTf}_2]$ and $[\text{C}_1^2\text{C}_1\text{Him}][\text{NTf}_2]$, which was performed in the temperature range from 328.15 to 343.15 K and 303.15 to 343.15 K, respectively, due to their higher melting temperature. The temperature of the ionic liquid in each surface tension measurement was considered to be the same than as measured inside the aluminum chamber with a Pt100 within ± 0.1 K placed at a distance of approximately 20 mm from the liquid drop. After reaching a specific temperature inside the aluminum chamber, the measurements were carried out after 40 min to guarantee the thermal stabilization. Silica gel was kept inside the air chamber to maintain a dry environment.

For the surface tension determination at each temperature, and for each ionic liquid, at least 5 drops were formed and analyzed. For each drop, an average of 150 images was captured. The analysis of the drop shape was done with the software modules SCA 20 where the gravitational acceleration ($g = 9.8018$ m s^{-2}) and latitude (lat. = 40°) were used according to the location of the assay. The surface tensions were calculated using the measured density data. Further details on the equipment and its validity to measure surface tensions of ILs were previously addressed.^{31–33}

3. RESULTS AND DISCUSSION

3.1. Thermal Behavior. The experimental results of the onset temperatures of glass, cold crystallization, and solid–solid and fusion transitions are presented in Table 2 along with some available literature data for comparison. The enthalpy measure-

ments of transitions were obtained by numerical integration of the peak thus obtained. Estimation errors of ± 0.5 K for the onset temperature and ± 0.7 kJ mol^{-1} for enthalpies were assumed taking into account the combined uncertainty of the calibration and the IL experiments. The values found in the literature concerning the phase behavior of the ionic liquids studied here are scarce and in poor agreement with each other.^{6,34–36} This discrepancy in the phase transitions comes from the fact that the process by which liquids are cooled to form a supercooled liquid and glasses affects the crystallization kinetics, crystal perfection/relaxation level, and, as a consequence, the experimental results.^{37–39} The differences in the glass transition temperatures, T_g , determined in this work and those reported in literature do not exceed 5 K, which may result from the different cooling rates applied in the formation of the glass.³⁷ The structural symmetry of a supercooled liquid and the molecular weight affect the glass transition.

Figure 1 depicts the glass transitions and fusion temperatures of the studied ILs. As expected, T_g increases with the molecular weight. The glass transition temperature of the $[\text{C}_{N-1}^3\text{C}_3\text{im}][\text{NTf}_2]$ series follows the order: $[\text{C}_1^3\text{C}_3\text{im}][\text{NTf}_2] < [\text{C}_2^3\text{C}_3\text{im}][\text{NTf}_2] < [\text{C}_3^3\text{C}_3\text{im}][\text{NTf}_2] < [\text{C}_4^3\text{C}_3\text{im}][\text{NTf}_2] < [\text{C}_5^3\text{C}_3\text{im}][\text{NTf}_2]$. The $[\text{C}_2^3\text{C}_3\text{im}][\text{NTf}_2]$ and $[\text{C}_3^3\text{C}_3\text{im}][\text{NTf}_2]$ have slightly lower T_g than their respective isomers. These results are consistent with the symmetric features. Liquids composed of asymmetric molecules form glasses much more readily than those consisting of symmetric ones.³⁸ Additionally, there is a correlation between the T_g and the viscosities measured in this work. The most viscous ILs are those with the highest T_g , which could be related with glass cohesive energy and their relation with their higher energy barrier to flow.

Among the short alkyl chain ILs with the acidic N–H group, only for $[\text{C}_1\text{Him}][\text{NTf}_2]$ it was not possible to obtain a glass transition temperature due to the fast and easy crystallization mechanism even at fast cooling rate before the glass formation. The fast and easy crystallization mechanism could be related with small hindrance effect and high cohesive energy due to the acidic N–H group on the crystallization process. The $[\text{C}_4^2\text{C}_1^3\text{C}_3\text{im}][\text{NTf}_2]$ isomer with a methylation in the position 2, C(2), presents a higher T_g than the $[\text{C}_{N-1}^3\text{C}_3\text{im}][\text{NTf}_2]$ series due to the hindrance effect of the $-\text{CH}_3$ that decreases the cation–anion dynamics as will be discussed below. On the other hand, the significant increase in the T_g in the $[\text{C}_2\text{Him}][\text{NTf}_2]$ should be related to the increase of the

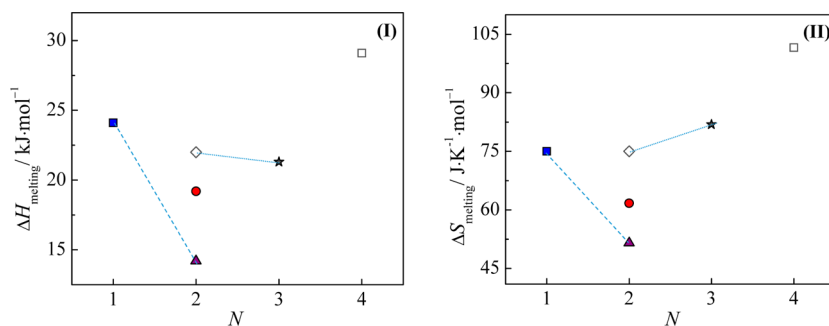


Figure 2. Graphic representation of the enthalpies (I) and entropies (II), as a function of the total number of carbon atoms in the alkyl side chains of the ILs, N : blue ■ - $[^1\text{C}_1\text{Him}][\text{NTf}_2]$; black ▲ - $[^1\text{C}_2\text{Him}][\text{NTf}_2]$; red ● - $[^1\text{C}_1^2\text{C}_1\text{Him}][\text{NTf}_2]$; ★ - $[^1\text{C}_2^3\text{C}_1\text{im}][\text{NTf}_2]$; ◇ - $[^1\text{C}_1^3\text{C}_1\text{im}][\text{NTf}_2]$; □ - $[^1\text{C}_2^3\text{C}_2\text{im}][\text{NTf}_2]$. The dashed and dotted lines highlight the $[^1\text{C}_N\text{Him}][\text{NTf}_2]$ and $[^1\text{C}_{N-1}^3\text{C}_1\text{im}][\text{NTf}_2]$ series which have no physical meaning.

cohesive energy due to the presence of the acidic N–H group. The empirical correlation between the T_g and T_m , $[T_g/T_m = 2/3]$, observed for polymers,⁴⁰ was also found here for the $[^1\text{C}_2\text{Him}][\text{NTf}_2]$ and $[^1\text{C}_2^3\text{C}_1\text{im}][\text{NTf}_2]$.

For the enthalpies and entropies of transitions, the results presented in this work show some deviations from the literature values.^{34,35} The entropy of transition was determined by the relation: $\Delta S_{\text{trans.}} = \Delta H_{\text{trans.}}/T_{\text{trans.}}$.

The discussion, comparison, and interpretation of the results with the literature data should be carried out with caution since the obtained of temperatures and enthalpies of transitions are affected by the thermal history and the methodology applied to the phase behavior studies (e.g., temperature scan rate, quenching procedure, time of stabilization, impurities, crucible material, and sample size).

Figure 2 depicts the enthalpies and entropies of melting as a function of the total number of carbon atoms, N , in the alkyl side chains of the ILs. The initial decrease in the enthalpy of melting is reflected in the initial decrease of the melting temperatures along the total number of carbons of the cation. The enthalpic differentiation between the series $[^1\text{C}_{N-1}^3\text{C}_1\text{im}][\text{NTf}_2]$ and $[^1\text{C}_N\text{Him}][\text{NTf}_2]$ is, however, partially canceled in the melting temperatures due to the entropic compensation. The higher temperature of melting of the $[^1\text{C}_1^2\text{C}_1\text{Him}][\text{NTf}_2]$ relative to the $[^1\text{C}_2\text{Him}][\text{NTf}_2]$ and $[^1\text{C}_1^3\text{C}_1\text{im}][\text{NTf}_2]$ isomers is ruled by the lower entropy of melting in agreement with the decrease of the anion–cation dynamics due to the methylation in the position 2, C(2), of the imidazolium ring. The melting temperature of the $[^1\text{C}_2^3\text{C}_2\text{im}][\text{NTf}_2]$ is similar to the $[^1\text{C}_1^3\text{C}_1\text{im}][\text{NTf}_2]$ besides their significantly higher enthalpy of melting, reflecting the strong entropic compensation effect.

3.2. Densities. The experimental raw data for density for the $[^1\text{C}_1\text{Him}][\text{NTf}_2]$, $[^1\text{C}_2\text{Him}][\text{NTf}_2]$, $[^1\text{C}_2^3\text{C}_3\text{im}][\text{NTf}_2]$, and $[^1\text{C}_1^2\text{C}_1\text{Him}][\text{NTf}_2]$ ILs are presented in the Supporting Information, Table SI.2. The density data (ρ), in the studied temperature (T) range, was further correlated using a second order polynomial equation:

$$\ln(\rho/\text{kg}\cdot\text{m}^{-3}) = a + b \cdot T + c \cdot T^2 \quad (1)$$

where a , b , and c are the coefficients obtained from the least-squares fitting of eq 1, and T is the temperature in K. The graphic representation of the logarithm of density as a function of the temperature is presented in Figure 3, together with literature data¹⁵ for $[^1\text{C}_{N-1}^3\text{C}_1\text{im}][\text{NTf}_2]$ (where $N = 3-6$) and $[^1\text{C}_{N/2}^3\text{C}_{N/2}\text{im}][\text{NTf}_2]$ (where $N = 2, 4, 6$).

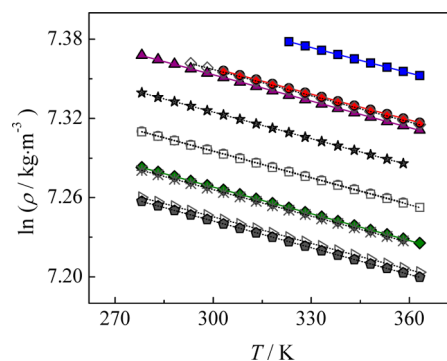


Figure 3. Logarithm of density as a function of temperature. This work: blue ■ - $[^1\text{C}_1\text{Him}][\text{NTf}_2]$; purple ▲ - $[^1\text{C}_2\text{Him}][\text{NTf}_2]$; red ● - $[^1\text{C}_1^2\text{C}_1\text{Him}][\text{NTf}_2]$; green ◆ - $[^1\text{C}_2^3\text{C}_3\text{im}][\text{NTf}_2]$; Literature:¹⁵ ★ - $[^1\text{C}_2^3\text{C}_1\text{im}][\text{NTf}_2]$; ○ - $[^1\text{C}_3^3\text{C}_1\text{im}][\text{NTf}_2]$; * - $[^1\text{C}_4^3\text{C}_1\text{im}][\text{NTf}_2]$; △ - $[^1\text{C}_5^3\text{C}_1\text{im}][\text{NTf}_2]$; ◇ - $[^1\text{C}_1^3\text{C}_1\text{im}][\text{NTf}_2]$; □ - $[^1\text{C}_2^3\text{C}_2\text{im}][\text{NTf}_2]$; black pentagon - $[^1\text{C}_3^3\text{C}_3\text{im}][\text{NTf}_2]$.

The isobaric thermal expansion coefficient, α_p , which considers the volumetric changes with temperature, was derived using eq 2:

$$\alpha_p = - \frac{1}{\rho} \left(\frac{\partial \rho}{\partial T} \right)_p = - \left(\frac{\partial \ln \rho}{\partial T} \right)_p = - [b + 2c \cdot (T/K)] \quad (2)$$

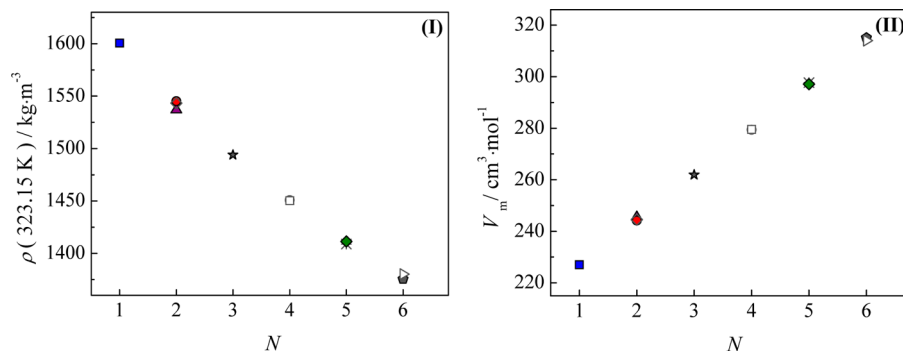
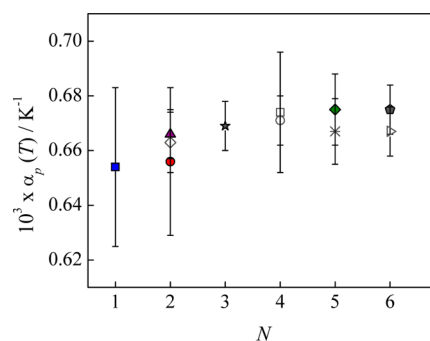
where ρ is the density in $\text{kg}\cdot\text{m}^{-3}$, T is the temperature in K, p is the standard pressure (0.1 MPa), and b and c are the fitting coefficients of eq 1. The fitting parameters such as the molar volume and the thermal expansion coefficients, at $T = 323.15$ K and 0.1 MPa, for all the studied ILs are listed in Table 3. Due to the fact that some of the ILs are solid at room temperature, the comparison of the data was done at $T = 323.15$ K.

The graphic representations of the density and molar volume and thermal expansion coefficients at 323.15 K and 0.1 MPa, against the total number of carbon atoms in the alkyl side chains of the cation, N , are presented in Figures 4 and 5, respectively. No significant differentiation in the isomers could be detected in the density and thermal expansion coefficients. Thus, it can be concluded that the volumetric properties are barely affected by the geometric and structural isomerization for these ILs, following a quite regular trend.

3.3. Viscosities. The experimental viscosity data for the $[^1\text{C}_1\text{Him}][\text{NTf}_2]$, $[^1\text{C}_2\text{Him}][\text{NTf}_2]$, $[^1\text{C}_2^3\text{C}_3\text{im}][\text{NTf}_2]$, and $[^1\text{C}_1^2\text{C}_1\text{Him}][\text{NTf}_2]$ ILs are presented in the Supporting Information, Table SI.3. Figure 6 depicts the graphic representation of the $\ln(\eta/\text{mPa}\cdot\text{s})$ against the temperature,

Table 3. List of the Fitted Parameters (eq 1), Density, Molar Volume, and the Thermal Expansion Coefficients, α_p , at 323.15 K and 0.1 MPa for the Studied ILs

ionic liquid	a	$10^4 \times b/K^{-1}$	$10^7 \times c/K^{-2}$	$T = 323.15 \text{ K}$		
				$\rho/(\text{kg}\cdot\text{m}^{-3})$	$V_m/(\text{cm}^3\cdot\text{mol}^{-1})$	$10^3 \times \alpha_p/K^{-1}$
$[\text{C}_1\text{Him}][\text{NTf}_2]$	7.6198 ± 0.0036	-8.42 ± 0.21	2.90 ± 0.30	1600.6	227.0	0.654 ± 0.029
$[\text{C}_2\text{Him}][\text{NTf}_2]$	7.5678 ± 0.0010	-7.59 ± 0.07	1.43 ± 0.10	1537.0	245.5	0.666 ± 0.009
$[\text{C}_2^3\text{C}_3\text{im}][\text{NTf}_2]$	7.4844 ± 0.0014	-7.62 ± 0.09	1.35 ± 0.14	1411.4	297.1	0.675 ± 0.013
$[\text{C}_1^2\text{C}_1\text{Him}][\text{NTf}_2]$	7.5632 ± 0.0032	-7.07 ± 0.19	0.79 ± 0.29	1545.2	244.2	0.656 ± 0.027

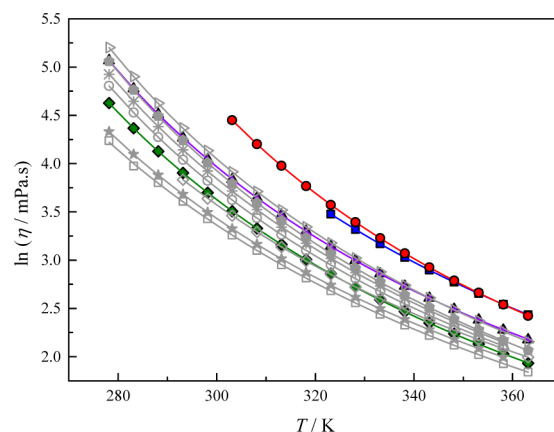
**Figure 4.** Density (I) and molar volume (II), at 323.15 K and 0.1 MPa, as a function of the total number of carbon atoms in the alkyl side chains of the cation, N . This work: blue ■ - $[\text{C}_1\text{Him}][\text{NTf}_2]$; purple ▲ - $[\text{C}_2\text{Him}][\text{NTf}_2]$; red ● - $[\text{C}_1^2\text{C}_1\text{Him}][\text{NTf}_2]$; green ◆ - $[\text{C}_2^3\text{C}_3\text{im}][\text{NTf}_2]$; Literature: ★ - $[\text{C}_2^3\text{C}_3\text{im}][\text{NTf}_2]$; ○ - $[\text{C}_3^3\text{C}_1\text{im}][\text{NTf}_2]$; * - $[\text{C}_4^3\text{C}_1\text{im}][\text{NTf}_2]$; △ - $[\text{C}_5^3\text{C}_1\text{im}][\text{NTf}_2]$; ◇ - $[\text{C}_1^3\text{C}_1\text{im}][\text{NTf}_2]$; □ - $[\text{C}_2^3\text{C}_2\text{im}][\text{NTf}_2]$; black pentagon - $[\text{C}_3^3\text{C}_3\text{im}][\text{NTf}_2]$.¹⁵**Figure 5.** Thermal expansion coefficient, α_p , at 323.15 K and 0.1 MPa, as a function of the total number of carbon atoms in the alkyl side chains of the cation, N . This work: blue ■ - $[\text{C}_1\text{Him}][\text{NTf}_2]$; purple ▲ - $[\text{C}_2\text{Him}][\text{NTf}_2]$; red ● - $[\text{C}_1^2\text{C}_1\text{Him}][\text{NTf}_2]$; green ◆ - $[\text{C}_2^3\text{C}_3\text{im}][\text{NTf}_2]$; Literature: ★ - $[\text{C}_2^3\text{C}_3\text{im}][\text{NTf}_2]$; ○ - $[\text{C}_3^3\text{C}_1\text{im}][\text{NTf}_2]$; * - $[\text{C}_4^3\text{C}_1\text{im}][\text{NTf}_2]$; △ - $[\text{C}_5^3\text{C}_1\text{im}][\text{NTf}_2]$; ◇ - $[\text{C}_1^3\text{C}_1\text{im}][\text{NTf}_2]$; □ - $[\text{C}_2^3\text{C}_2\text{im}][\text{NTf}_2]$; black pentagon - $[\text{C}_3^3\text{C}_3\text{im}][\text{NTf}_2]$.¹⁵

together with literature data for $[\text{C}_{N-1}^3\text{C}_1\text{im}][\text{NTf}_2]$ (where $N = 3-6$) and $[\text{C}_{N/2}^3\text{C}_{N/2}\text{im}][\text{NTf}_2]$ (where $N = 2, 4, 6$) series.^{15,41}

The experimental viscosity data was correlated using the Vogel–Tammann–Fulcher (VTF) model described in eq 3:

$$\ln(\eta/\text{mPa}\cdot\text{s}) = \ln(A_\eta/\text{mPa}\cdot\text{s}) + \frac{B_\eta}{(T - C_\eta)} \quad (3)$$

where η is the viscosity in $\text{mPa}\cdot\text{s}$, T is the temperature in K, and A_η , B_η , and C_η are the fitting parameters from the fitting of the experimental data. The energy barrier of the fluid to a shear stress was evaluated based on the viscosity dependence with the temperature using eq 4

**Figure 6.** Logarithm of viscosity as a function of temperature for studied ILs. The solid lines represent the Vogel–Tammann–Fulcher fitting from eq 3. This work: blue ■ - $[\text{C}_1\text{Him}][\text{NTf}_2]$; purple ▲ - $[\text{C}_2\text{Him}][\text{NTf}_2]$; red ● - $[\text{C}_1^2\text{C}_1\text{Him}][\text{NTf}_2]$; green ◆ - $[\text{C}_2^3\text{C}_3\text{im}][\text{NTf}_2]$; Literature: ★ - $[\text{C}_2^3\text{C}_3\text{im}][\text{NTf}_2]$; ○ - $[\text{C}_3^3\text{C}_1\text{im}][\text{NTf}_2]$; * - $[\text{C}_4^3\text{C}_1\text{im}][\text{NTf}_2]$; △ - $[\text{C}_5^3\text{C}_1\text{im}][\text{NTf}_2]$; ◇ - $[\text{C}_1^3\text{C}_1\text{im}][\text{NTf}_2]$; □ - $[\text{C}_2^3\text{C}_2\text{im}][\text{NTf}_2]$; black pentagon - $[\text{C}_3^3\text{C}_3\text{im}][\text{NTf}_2]$.^{15,41}

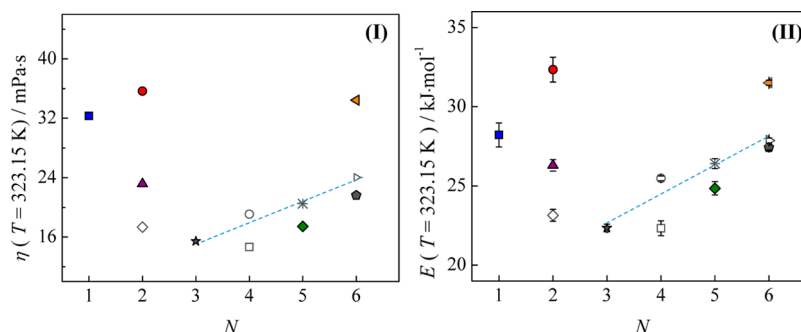
$$E = R \cdot \frac{\partial(\ln \eta)}{\partial(1/T)} = R \cdot \left(\frac{B_\eta}{\left(\frac{C_\eta^2}{T^2} - \frac{2 \cdot C_\eta}{T} + 1 \right)} \right) \quad (4)$$

The derived coefficients of the VTF eq 3, the viscosity and the derived energy barrier, E , at $T = 323.15 \text{ K}$, for the studied ILs, are presented in Table 4.

The graphic representation of viscosity, η , at $T = 323.15 \text{ K}$, as a function of the total number of carbon atoms in the alkyl chains in the cation, for the $[\text{C}_1\text{Him}][\text{NTf}_2]$, $[\text{C}_2\text{Him}][\text{NTf}_2]$, $[\text{C}_2^3\text{C}_3\text{im}][\text{NTf}_2]$, and $[\text{C}_1^2\text{C}_1\text{Him}][\text{NTf}_2]$ ILs and

Table 4. Fitting Parameters of VTF Equation for the Viscosity Data of the Studied ILs, Viscosity, and the Derived Energy Barrier at $T = 323.15$ K

ionic liquid	$A_\eta/(\text{mPa}\cdot\text{s})$	B_η/K	C_η/K	$T = 323.15$ K	
				$\eta/(\text{mPa}\cdot\text{s})$	$E/(\text{kJ}\cdot\text{mol}^{-1})$
$[\text{C}_1\text{Him}][\text{NTf}_2]$	0.177 ± 0.005	833 ± 9	163.0 ± 1.0	32.31	28.22 ± 0.76
$[\text{C}_2\text{Him}][\text{NTf}_2]$	0.214 ± 0.004	724 ± 5	168.5 ± 0.5	23.15	26.30 ± 0.36
$[\text{C}_2^3\text{C}_3\text{im}][\text{NTf}_2]$	0.150 ± 0.003	789 ± 7	157.1 ± 0.6	17.43	24.85 ± 0.42
$[\text{C}_1^2\text{C}_1\text{Him}][\text{NTf}_2]$	0.234 ± 0.005	678 ± 6	188.2 ± 0.6	35.66	32.34 ± 0.78

**Figure 7.** Viscosity ($\eta/\text{mPa}\cdot\text{s}$) at $T = 323.15$ K and 0.1 MPa (I) and energy barrier ($E/\text{kJ}\cdot\text{mol}^{-1}$) at 323.15 K (II) for ILs under study as a function of the total number of carbons, N . This work: blue ■ - $[\text{C}_1\text{Him}][\text{NTf}_2]$; purple ▲ - $[\text{C}_2\text{Him}][\text{NTf}_2]$; red ● - $[\text{C}_1^2\text{C}_1\text{Him}][\text{NTf}_2]$; green ◆ - $[\text{C}_2^3\text{C}_3\text{im}][\text{NTf}_2]$; Literature: ★ - $[\text{C}_2^3\text{C}_3\text{im}][\text{NTf}_2]$; ○ - $[\text{C}_3^3\text{C}_3\text{im}][\text{NTf}_2]$; * - $[\text{C}_4^3\text{C}_3\text{im}][\text{NTf}_2]$; △ - $[\text{C}_5^3\text{C}_3\text{im}][\text{NTf}_2]$; ◇ - $[\text{C}_1^3\text{C}_1\text{im}][\text{NTf}_2]$; □ - $[\text{C}_2^3\text{C}_2\text{im}][\text{NTf}_2]$; black pentagon - $[\text{C}_3^3\text{C}_3\text{im}][\text{NTf}_2]$;^{15,41} orange ▲ - $[\text{C}_4^2\text{C}_1^3\text{C}_1\text{im}][\text{NTf}_2]$.⁴² The dashed lines highlight the $[\text{C}_{N-1}^3\text{C}_1\text{im}][\text{NTf}_2]$ series, which has no physical meaning.**Table 5. Number of Drop Experiments, N_{drop} , the Molar Heat Capacity, $C_{p,m}^\circ$ ($\text{J}\cdot\text{K}^{-1}\cdot\text{mol}^{-1}$), Specific Heat Capacities, C_p° ($\text{J}\cdot\text{K}^{-1}\cdot\text{g}^{-1}$), and Volumic Heat Capacities, C_p°/V ($\text{J}\cdot\text{K}^{-1}\cdot\text{cm}^{-3}$) at 298.15 K**

ionic liquid	N_{drop}	$C_{p,m}^\circ/\text{J}\cdot\text{K}^{-1}\cdot\text{mol}^{-1}$	$C_p^\circ/\text{J}\cdot\text{K}^{-1}\cdot\text{g}^{-1}$	$(C_p^\circ/V)/\text{J}\cdot\text{K}^{-1}\cdot\text{cm}^{-3}$
$[\text{C}_1\text{Him}][\text{NTf}_2]$ (cr)	12	441.64 ± 0.33	1.2158 ± 0.0009	1.9785 ± 0.0015
$[\text{C}_2\text{Him}][\text{NTf}_2]$ (l)	33	484.08 ± 0.44	1.2831 ± 0.0012	2.0055 ± 0.0019
$[\text{C}_2^3\text{C}_3\text{im}][\text{NTf}_2]$ (l)	19	565.08 ± 0.57	1.3475 ± 0.0014	1.9342 ± 0.0020
$[\text{C}_1^2\text{C}_1\text{Him}][\text{NTf}_2]$ (l)	23	483.08 ± 0.38	1.2804 ± 0.0010	2.0113 ± 0.0016

their comparison with the literature data^{15,41} for the $[\text{C}_{N-1}^3\text{C}_1\text{im}][\text{NTf}_2]$ (where $N = 3-6$) and $[\text{C}_{N/2}^3\text{C}_{N/2}\text{im}][\text{NTf}_2]$ (where $N = 2, 4, 6$) series is depicted in Figure 7(I). The energy barrier at $T = 323.15$ K, E ($T = 323.15$ K), as a function of the total number of carbon atoms in the alkyl side chains of the cation, N , is presented in Figure 7(II).

The $[\text{C}_{N-1}^3\text{C}_1\text{im}][\text{NTf}_2]$ series is systematically more viscous than the $[\text{C}_{N/2}^3\text{C}_{N/2}\text{im}][\text{NTf}_2]$ series, as described in a previous work.¹⁵ A strong differentiation in the viscosities of the isomers with short alkyl chains, such as $[\text{C}_2\text{Him}][\text{NTf}_2]$, $[\text{C}_1^2\text{C}_1\text{Him}][\text{NTf}_2]$, and $[\text{C}_1^3\text{C}_1\text{im}][\text{NTf}_2]$ was observed. The shorter alkyl substituted ILs present higher viscosities when compared with the long alkyl chain series. This trend of the viscosity along the total number of carbons of the cation is very similar to that observed in the energy barrier profile, as depicted in Figure 7, which is an indication that the viscosity trend is ruled by the differentiation in the cohesive energy. The most viscous ILs, $[\text{C}_1\text{Him}][\text{NTf}_2]$, $[\text{C}_2\text{Him}][\text{NTf}_2]$, and $[\text{C}_1^2\text{C}_1\text{Him}][\text{NTf}_2]$, have an acidic N–H group in the imidazolium ring. The acidic hydrogen atom is able to establish hydrogen bonds with the oxygen atoms of the $[\text{NTf}_2]^-$ anion, leading to an increase of energy barrier of shear stress. The analysis of the IR spectra of the $[\text{C}_1^3\text{C}_1\text{im}][\text{NTf}_2]$, $[\text{C}_1^2\text{C}_1\text{Him}][\text{NTf}_2]$, and $[\text{C}_1\text{Him}][\text{NTf}_2]$ (data is presented in Supporting Information) in the range of $400-4000\text{ cm}^{-1}$ do not show any significant differentiation that could be associated with a change in the sulfonyl vibrations; however, the

enhancement of the anion–cation interaction by increasing the number and the strength of H-bond abilities was previously proposed by Ludwig et al.⁴³ based on FIR (far IR) spectroscopy in agreement with our conclusion and remarks concerning the effect of the acid N–H group in the thermophysical properties.

The effect of methylation of the C(2) position in the viscosity was previously discussed by Hunt,¹⁷ based on computational studies, considering the reduction of ion-pair configurational variation, which leads to an additional increase of the energy barrier in relation to other isomers, as observed in this work. Our results also indicate the differentiation (increase) in the viscosity by the methylation in C(2) in the $[\text{C}_4^2\text{C}_1^3\text{C}_1\text{im}][\text{NTf}_2]$ with the same magnitude that was observed in $[\text{C}_1^2\text{C}_1\text{Him}][\text{NTf}_2]$, giving thus additional support for the previous rationalization concerning the effect of the substitution in the position 2 of the imidazolium.

3.4. Heat Capacities. The molar, $C_{p,m}^\circ$ ($\text{J}\cdot\text{K}^{-1}\cdot\text{mol}^{-1}$), specific, C_p° ($\text{J}\cdot\text{K}^{-1}\cdot\text{g}^{-1}$), and volumetric, C_p°/V ($\text{J}\cdot\text{K}^{-1}\cdot\text{cm}^{-3}$) heat capacities at $T = 298.15$ K and 0.1 MPa, of the $[\text{C}_1\text{Him}][\text{NTf}_2]$, $[\text{C}_2\text{Him}][\text{NTf}_2]$, $[\text{C}_2^3\text{C}_3\text{im}][\text{NTf}_2]$, and $[\text{C}_1^2\text{C}_1\text{Him}][\text{NTf}_2]$ ILs are presented in Table 5 together with the total number of drop experiments, N_{drop} for each ionic liquid. Due to the high metastability of the supercooled liquid $[\text{C}_1^2\text{C}_1\text{Him}][\text{NTf}_2]$, it was possible to measure the heat capacity in the liquid phase, which is also presented in Table 5.

The heat capacity data obtained for the $[\text{C}_1\text{Him}][\text{NTf}_2]$, $[\text{C}_2\text{Him}][\text{NTf}_2]$, $[\text{C}_2^3\text{C}_3\text{im}][\text{NTf}_2]$, and $[\text{C}_1^2\text{C}_1\text{Him}][\text{NTf}_2]$

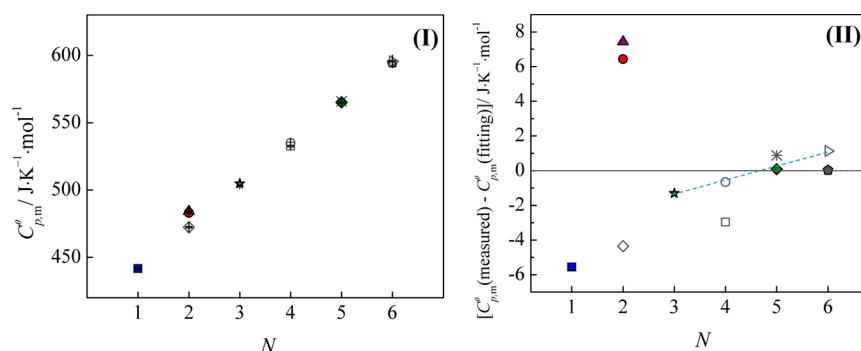


Figure 8. Molar heat capacities, at 298.15 K, as a function of the total number of carbon atoms in the alkyl side chains of the cation, N (I): blue ■ - $[\text{C}_1\text{Him}][\text{NTf}_2]$ (cr); purple ▲ - $[\text{C}_2\text{Him}][\text{NTf}_2]$; red ● - $[\text{C}_1\text{C}_2\text{Him}][\text{NTf}_2]$; green ◆ - $[\text{C}_1\text{C}_3\text{C}_3\text{im}][\text{NTf}_2]$; Literature: ★ - $[\text{C}_2\text{C}_3\text{C}_1\text{im}][\text{NTf}_2]$; ○ - $[\text{C}_1\text{C}_3\text{C}_1\text{im}][\text{NTf}_2]$; * - $[\text{C}_1\text{C}_4\text{C}_1\text{im}][\text{NTf}_2]$; △ - $[\text{C}_1\text{C}_5\text{C}_1\text{im}][\text{NTf}_2]$; ⁴⁴ ◇ - $[\text{C}_1\text{C}_1\text{C}_3\text{C}_1\text{im}][\text{NTf}_2]$; □ - $[\text{C}_1\text{C}_2\text{C}_2\text{im}][\text{NTf}_2]$; black pentagon - $[\text{C}_1\text{C}_3\text{C}_3\text{im}][\text{NTf}_2]$.⁴⁵ Deviation from the $C_{p,m}^0$ (linear fitting) of the ILs presented in (I) as a function of total number of carbons in the alkyl side chains of the cation (II). The dashed lines highlight the $[\text{C}_{N-1}\text{C}_1\text{im}][\text{NTf}_2]$ series, which has no physical meaning.

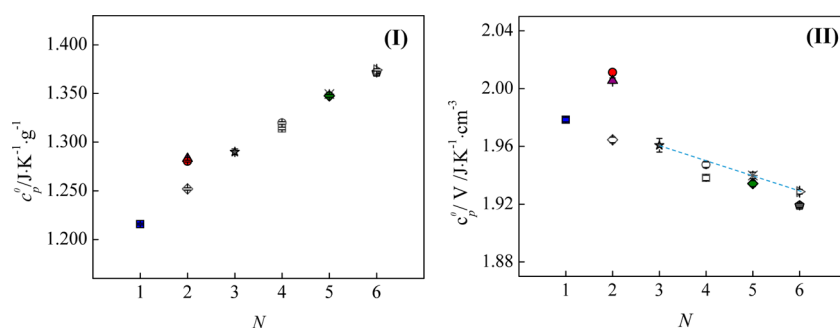


Figure 9. Specific heat capacities (I) and the volumetric heat capacities (II), at 298.15 K, as a function of the total number of carbon atoms in the alkyl side chains of the cation, N . blue ■ - $[\text{C}_1\text{Him}][\text{NTf}_2]$ (cr); purple ▲ - $[\text{C}_2\text{Him}][\text{NTf}_2]$; red ● - $[\text{C}_1\text{C}_2\text{Him}][\text{NTf}_2]$; green ◆ - $[\text{C}_1\text{C}_3\text{C}_3\text{im}][\text{NTf}_2]$; Literature: ★ - $[\text{C}_2\text{C}_3\text{C}_1\text{im}][\text{NTf}_2]$; ○ - $[\text{C}_1\text{C}_3\text{C}_1\text{im}][\text{NTf}_2]$; * - $[\text{C}_1\text{C}_4\text{C}_1\text{im}][\text{NTf}_2]$; △ - $[\text{C}_1\text{C}_5\text{C}_1\text{im}][\text{NTf}_2]$; ⁴⁴ ◇ - $[\text{C}_1\text{C}_1\text{C}_3\text{C}_1\text{im}][\text{NTf}_2]$; □ - $[\text{C}_1\text{C}_2\text{C}_2\text{im}][\text{NTf}_2]$; black pentagon - $[\text{C}_1\text{C}_3\text{C}_3\text{im}][\text{NTf}_2]$.⁴⁵ The dashed lines highlight the $[\text{C}_{N-1}\text{C}_1\text{im}][\text{NTf}_2]$ series, which has no physical meaning.

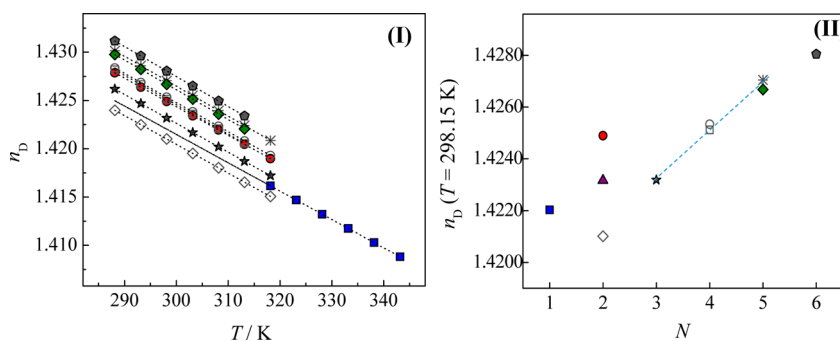


Figure 10. Refractive indices as a function of temperature for studied ILs (I): Refractive indices, n_D ($T = 298.15 \text{ K}$) as a function of the total number of carbon atoms in the alkyl side chains of the cation, N (II). blue ■ - $[\text{C}_1\text{Him}][\text{NTf}_2]$; purple ▲ - $[\text{C}_2\text{Him}][\text{NTf}_2]$; red ● - $[\text{C}_1\text{C}_2\text{Him}][\text{NTf}_2]$; green ◆ - $[\text{C}_1\text{C}_3\text{C}_3\text{im}][\text{NTf}_2]$; ★ - $[\text{C}_2\text{C}_3\text{C}_1\text{im}][\text{NTf}_2]$; ○ - $[\text{C}_1\text{C}_3\text{C}_1\text{im}][\text{NTf}_2]$; * - $[\text{C}_1\text{C}_4\text{C}_1\text{im}][\text{NTf}_2]$; ◇ - $[\text{C}_1\text{C}_1\text{C}_3\text{C}_1\text{im}][\text{NTf}_2]$; □ - $[\text{C}_1\text{C}_2\text{C}_2\text{im}][\text{NTf}_2]$; black pentagon - $[\text{C}_1\text{C}_3\text{C}_3\text{im}][\text{NTf}_2]$. The dashed lines highlight the $[\text{C}_{N-1}\text{C}_1\text{im}][\text{NTf}_2]$ series which has no physical meaning.

was compared with the data for the $[\text{C}_{N-1}\text{C}_1\text{im}][\text{NTf}_2]$ (where $N = 3-5$) and $[\text{C}_{N/2}\text{C}_{N/2}\text{im}][\text{NTf}_2]$ (where $N = 2, 4, 6$) ILs available in the literature.^{44,45} Figure 8 (I) shows the representation of the molar heat capacity data ($C_{p,m}^0$) against the total number of carbon atoms in the alkyl side chains of the cation, N , of the $[\text{C}_1\text{Him}][\text{NTf}_2]$, $[\text{C}_2\text{Him}][\text{NTf}_2]$, $[\text{C}_1\text{C}_2\text{C}_3\text{im}][\text{NTf}_2]$, and $[\text{C}_1\text{C}_1\text{C}_2\text{Him}][\text{NTf}_2]$ ILs, together with the data for the $[\text{C}_{N-1}\text{C}_1\text{im}][\text{NTf}_2]$ (where $N = 3-5$)⁴⁴ and $[\text{C}_{N/2}\text{C}_{N/2}\text{im}][\text{NTf}_2]$ (where $N = 2, 4, 6$)⁴⁵ and (II) the deviation from the linear fitting of the molar heat capacities. Figure 9 presents the plots of the specific heat capacity (I) and

the volumetric heat capacities (II) against the total number of carbon atoms in the alkyl side chains of the cation, N , of the considered ILs.

From Figure 8 (II) it can be seen that the $N = 2$ isomers, namely, $[\text{C}_2\text{Him}][\text{NTf}_2]$ $[\text{C}_1\text{C}_2\text{Him}][\text{NTf}_2]$, are outliers, with a significant positive deviation from the linear trend of the ILs series presented in this work. From the analysis of the volumetric heat capacities depicted in Figure 9 (II), the differentiation is more evident. The heat capacity per volume units is significantly higher for the $[\text{C}_2\text{Him}][\text{NTf}_2]$ and $[\text{C}_1\text{C}_2\text{Him}][\text{NTf}_2]$. The presence of the acidic N—H

contributes to a significant interaction potential profile which leads to a heat capacity increment of $\sim 12 \text{ J K}^{-1} \text{ mol}^{-1}$. In agreement with the previous findings, the $[\text{C}_2^3\text{C}_2\text{im}][\text{NTf}_2]$ (symmetrical series) presents a slightly lower heat capacity than the asymmetric series.⁴⁵ However, the $[\text{C}_2^3\text{C}_3\text{im}][\text{NTf}_2]$ nicely fits the trend of the asymmetric series, as expected.

3.5. Refractive Indices. The refractive indices fitting data for $[\text{C}_1\text{Him}][\text{NTf}_2]$, $[\text{C}_2\text{Him}][\text{NTf}_2]$, $[\text{C}_2^3\text{C}_3\text{im}][\text{NTf}_2]$, $[\text{C}_1^2\text{C}_1\text{Him}][\text{NTf}_2]$, $[\text{C}_{N-1}^3\text{C}_1\text{im}][\text{NTf}_2]$ (where $N = 3-6$), and $[\text{C}_{N/2}^3\text{C}_{N/2}\text{im}][\text{NTf}_2]$ (where $N = 2, 4, 6$), in the temperature range from 289 to 342 K, are presented in Supporting Information, Table SI.4. The graphic representation of the refractive indices, as a function of the temperature for the studied ILs, is depicted in Figure 10 (I). Table 6 lists the

Table 6. Experimental Refractive Indices at the Sodium D-Line, n_D^b , for the Studied ILs as a Function of Temperature T at 0.1 MPa^a

ionic liquid	n_D (298.15 K)	$10^4 \cdot (dn_D/dT) / \text{K}^{-1}$	n_D (298.15 K) Literature
$[\text{C}_1\text{Him}][\text{NTf}_2]$	1.42203	-2.93 ± 0.01	n.a.
$[\text{C}_2\text{Him}][\text{NTf}_2]$	1.42317	-3.012 ± 0.002	n.a.
$[\text{C}_1^2\text{C}_1\text{Him}][\text{NTf}_2]$	1.42490	-2.959 ± 0.003	n.a.
$[\text{C}_1^3\text{C}_1\text{im}][\text{NTf}_2]$	1.42101	-2.97 ± 0.02	n.a.
$[\text{C}_2^3\text{C}_1\text{im}][\text{NTf}_2]$	1.42319	-2.99 ± 0.01	1.4230(9) ⁵⁸ 1.4220 ⁴⁷ 1.42251 ⁴⁸ 1.42307 ⁴⁹⁻⁵¹ 1.42298 ⁵² 1.42525 ⁵³
$[\text{C}_3^3\text{C}_1\text{im}][\text{NTf}_2]$	1.42534	-3.02 ± 0.01	1.42525 ⁵³
$[\text{C}_2^3\text{C}_2\text{im}][\text{NTf}_2]$	1.42512	-3.04 ± 0.02	n.a.
$[\text{C}_2^3\text{C}_3\text{im}][\text{NTf}_2]$	1.42668	-3.08 ± 0.01	n.a.
$[\text{C}_4^3\text{C}_1\text{im}][\text{NTf}_2]$	1.42705	-3.10 ± 0.01	1.42653 ⁴⁸ 1.42692 ^{54,55} 1.427 ⁵⁶ 1.451 ⁵⁷ 1.42672 ^{50,51}
$[\text{C}_3^3\text{C}_3\text{im}][\text{NTf}_2]$	1.42805	-3.10 ± 0.01	n.a.

^aAvailable literature data at $T = 298.15 \text{ K}$. ^bIn the temperature interval, n_D , at a specific temperature, T , can be estimated using the following equation: $n_D(T/K) = n_D(298.15 \text{ K}) + dn_D/dT \cdot (T/K - 298.15 \text{ K})$.

refractive indices of all studied ILs, at $T = 298.15 \text{ K}$, together with available literature values, and the temperature derivative of the temperature dependence of the refractive index, dn_D/dT . The plots of the refractive indices, at $T = 298.15 \text{ K}$, as a function of the total number of carbon atoms in the alkyl chains in the imidazolium cations, for the measured ILs, are shown in Figure 10 (II). The refractive indices obtained in this work are

in good agreement with the available literature values, with relative deviations under 2%.⁴⁶⁻⁵⁷

As shown in Figure 10 (II), the ILs with shorter alkyl chain length are clearly differentiated with respect to long-chain isomers. A regular increasing trend in the refractive indices from $[\text{C}_{N-1}^3\text{C}_1\text{im}][\text{NTf}_2]$ (where $N = 3-6$) and $[\text{C}_{N/2}^3\text{C}_{N/2}\text{im}][\text{NTf}_2]$ (where $N = 2, 4, 6$) was observed. Concerning the short alkyl chain ILs, the following order for the refractive indices was found: $[\text{C}_1^2\text{C}_1\text{Him}][\text{NTf}_2] > [\text{C}_2\text{Him}][\text{NTf}_2] > [\text{C}_1^3\text{C}_1\text{im}][\text{NTf}_2]$. The methylation in the C(2) position, as well as the N-H acidic group in the imidazolium ring, contributes to a significant differentiation in the cation-anion interactions which is reflected in their charge distribution and polarizability compared with their respective isomers.

3.6. Surface Tension. The surface thermodynamic properties, namely, surface entropy and surface enthalpy, were estimated using the quasi-linear dependence of the surface tension with temperature.⁵⁹

The surface entropy, $S'(T)$, was evaluated according to eq 5

$$S'(T) = -\left(\frac{d\gamma}{dT}\right)_T \quad (5)$$

whereas the surface enthalpy, $H'(T)$, was determined according to eq 6

$$H'(T) = \gamma - T\left(\frac{d\gamma}{dT}\right)_T \quad (6)$$

where γ stands for the surface tension and T for the temperature.

The values of the surface tensions and the thermodynamic functions, at $T = 330 \text{ K}$, of all the bis[(trifluoromethyl)sulfonyl]imide based ILs derived from the temperature dependence of the surface tension, $\gamma = f(T)$, in combination with the associated deviation⁶⁰ are presented in Table 7. Figure 11 depicts the dependence of the surface tension with temperature among the ILs. The experimental raw data for the ILs studied is presented in the Supporting Information, Table SI.5. The surface tension, at $T = 330 \text{ K}$, as a function of the total number of carbons is depicted in Figure 12. A strong differentiation in the surface tension between the $N = 2$ isomers was found to follow the trend: $[\text{C}_1^2\text{C}_1\text{im}][\text{NTf}_2] > [\text{C}_1^3\text{C}_1\text{im}][\text{NTf}_2] > [\text{C}_2\text{Him}][\text{NTf}_2]$.

The derived surface enthalpies and entropies of the ILs series are depicted in Figure 13. The higher values of surface tension of $[\text{C}_1^2\text{C}_1\text{Him}][\text{NTf}_2]$ and $[\text{C}_1^3\text{C}_1\text{im}][\text{NTf}_2]$ are in agreement with their higher interaction potential in the bulk. It is interesting to note that the present behavior reflects the low basicity of the bistriflamide where the full aprotic character of this ionic liquid is preserved even with the acidic N-H group

Table 7. Values of the Surface Tension γ (mN·m⁻¹) at 330.0 K, and Surface Thermodynamic Functions S' (J·K⁻¹·m⁻²) and H' (J·m⁻²)

ionic liquid	γ (330 K)/mN·m ⁻¹	$(S' \pm \sigma^a) \times 10^5 / (\text{J} \cdot \text{K}^{-1} \cdot \text{m}^{-2})$	$(H' \pm \sigma^a) \times 10^2 / (\text{J} \cdot \text{m}^{-2})$
$[\text{C}_1\text{Him}][\text{NTf}_2]$	36.2	5.1 ± 0.5	5.3 ± 0.2
$[\text{C}_2\text{Him}][\text{NTf}_2]$	33.1	5.5 ± 0.2	5.13 ± 0.08
$[\text{C}_2^3\text{C}_3\text{im}][\text{NTf}_2]$	32.0	4.6 ± 0.1	4.71 ± 0.02
$[\text{C}_1^2\text{C}_1\text{Him}][\text{NTf}_2]$	36.7	6.2 ± 0.1	5.73 ± 0.04
$[\text{C}_4^3\text{C}_1\text{im}][\text{NTf}_2]$	32.7	5.0 ± 0.1	4.91 ± 0.03

^aStandard deviation.

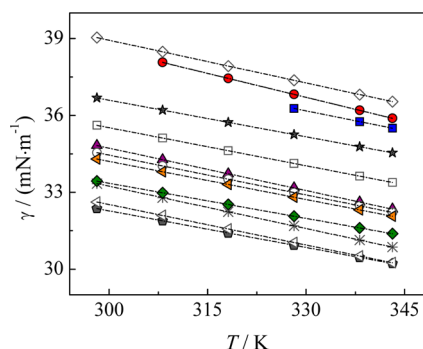


Figure 11. Surface tension values for the ILs as a function of temperature: blue ■ - $[^1\text{C}_1\text{Him}][\text{NTf}_2]$; purple ▲ - $[^1\text{C}_2\text{Him}][\text{NTf}_2]$; red ● - $[^1\text{C}_1^2\text{C}_1\text{Him}][\text{NTf}_2]$; green ◆ - $[^1\text{C}_2^3\text{C}_1\text{im}][\text{NTf}_2]$; orange ▲ - $[^1\text{C}_4^2\text{C}_1^3\text{C}_1\text{im}][\text{NTf}_2]$; Literature: ★ - $[^1\text{C}_2^3\text{C}_1\text{im}][\text{NTf}_2]$; ○ - $[^1\text{C}_3^3\text{C}_1\text{im}][\text{NTf}_2]$; * - $[^1\text{C}_4^3\text{C}_1\text{im}][\text{NTf}_2]$; △ - $[^1\text{C}_5^3\text{C}_1\text{im}][\text{NTf}_2]$; 61 ◇ - $[^1\text{C}_1^3\text{C}_1\text{im}][\text{NTf}_2]$; □ - $[^1\text{C}_2^3\text{C}_2\text{im}][\text{NTf}_2]$; black pentagon - $[^1\text{C}_3^3\text{C}_3\text{im}][\text{NTf}_2]$.¹³

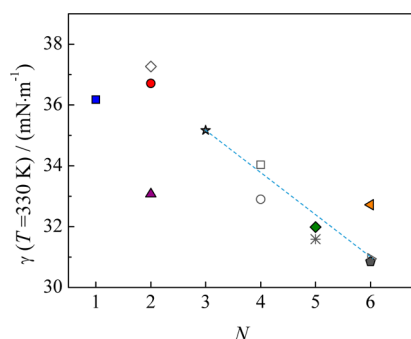


Figure 12. Surface tension dependence, at 330 K, as a function of the total number of carbons in the aliphatic chains, N . blue ■ - $[^1\text{C}_1\text{Him}][\text{NTf}_2]$; purple ▲ - $[^1\text{C}_2\text{Him}][\text{NTf}_2]$; red ● - $[^1\text{C}_1^2\text{C}_1\text{Him}][\text{NTf}_2]$; green ◆ - $[^1\text{C}_2^3\text{C}_1\text{im}][\text{NTf}_2]$; orange ▲ - $[^1\text{C}_4^2\text{C}_1^3\text{C}_1\text{im}][\text{NTf}_2]$; Literature data: ◇ - $[^1\text{C}_1^3\text{C}_1\text{im}][\text{NTf}_2]$; □ - $[^1\text{C}_2^3\text{C}_2\text{im}][\text{NTf}_2]$; black pentagon - $[^1\text{C}_3^3\text{C}_3\text{im}][\text{NTf}_2]$; 13 ★ - $[^1\text{C}_2^3\text{C}_1\text{im}][\text{NTf}_2]$; ○ - $[^1\text{C}_3^3\text{C}_1\text{im}][\text{NTf}_2]$; * - $[^1\text{C}_4^3\text{C}_1\text{im}][\text{NTf}_2]$; △ - $[^1\text{C}_5^3\text{C}_1\text{im}][\text{NTf}_2]$.⁶¹ The dashed line highlights the $[^1\text{C}_{N-1}^3\text{C}_1\text{im}][\text{NTf}_2]$ series, which has no physical meaning.

when compared with the recent results concerning the acetate derivatives.³² The remaining isomers follow a regular trend as observed previously,¹³ with an initial decrease of the surface

tension until $N = 6$, critical alkyl chain length (CAL), reflecting the decrease of the polar interaction.

3.7. Final Remarks. This work presents an extended study of the isomerization effect in the physicochemical properties of short chain length imidazolium $[\text{NTf}_2]^-$ ionic liquid series. A strong differentiation in the physicochemical properties arising from the presence of the acidic group, N–H, as well the methylation of position 2, C(2), in the imidazolium ring was found and interpreted. The observed differentiation of $[^1\text{C}_1\text{Him}][\text{NTf}_2]$, the isomers $[^1\text{C}_1^2\text{C}_1\text{Him}][\text{NTf}_2]$, $[^1\text{C}_2\text{Him}][\text{NTf}_2]$, and $[^1\text{C}_4^2\text{C}_1^3\text{C}_1\text{im}][\text{NTf}_2]$, when compared with the regular trend of the remaining IL member series, is in agreement with their higher interaction potential in the bulk. This increase in the interaction potential arises from two main effects, which contribute in the same direction to the differentiation: the acidic hydrogen N–H, that is able to form hydrogen bonds with the oxygen atoms of the $[\text{NTf}_2]^-$ anion; and the methylation in the C(2), which reduces the ion-pair configurational variation, leading to a more localized charge distribution and a significant decrease of the entropy of the liquid phase in agreement with the observed lower enthalpy of melting. The obtained results, and especially their comparative analysis, are in full agreement with the rationalization based on the higher interaction potential: higher heat capacities, higher viscosities, higher refractive indices, thermal behavior, and the bulk structuration derived from the surface tension results.

■ ASSOCIATED CONTENT

📄 Supporting Information

Compound names and purity data, density data, viscosity data, refractive indices data, surface tension data, FTIR data. The Supporting Information is available free of charge on the ACS Publications website at DOI: 10.1021/acs.jpcb.5b05354.

■ AUTHOR INFORMATION

Corresponding Author

*E-mail: lbsantos@fc.up.pt.

Notes

The authors declare no competing financial interest.

■ ACKNOWLEDGMENTS

Thanks are due to Fundação para a Ciência e Tecnologia (FCT), Lisbon, Portugal and to FEDER for financial support to Centro de Investigação em Química, University of Porto through the project Pest-C/QUI/UI0081/2013, and CICECO

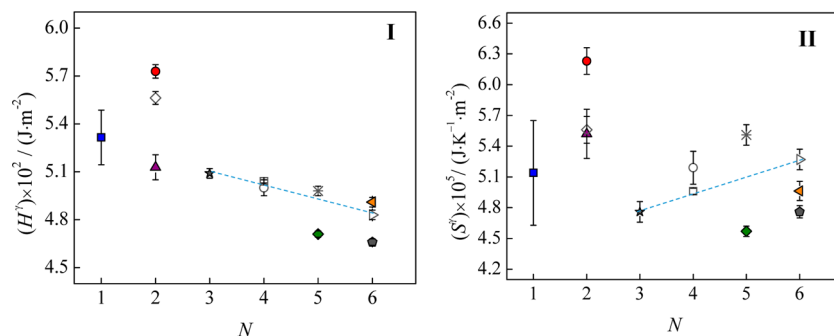


Figure 13. Surface enthalpies (I) and entropies (II) as a function of the total number of carbon atoms N , blue ■ - $[^1\text{C}_1\text{Him}][\text{NTf}_2]$; purple ▲ - $[^1\text{C}_2\text{Him}][\text{NTf}_2]$; red ● - $[^1\text{C}_1^2\text{C}_1\text{Him}][\text{NTf}_2]$; green ◆ - $[^1\text{C}_2^3\text{C}_1\text{im}][\text{NTf}_2]$; orange ▲ - $[^1\text{C}_4^2\text{C}_1^3\text{C}_1\text{im}][\text{NTf}_2]$; Literature data: ◇ - $[^1\text{C}_1^3\text{C}_1\text{im}][\text{NTf}_2]$; □ - $[^1\text{C}_2^3\text{C}_2\text{im}][\text{NTf}_2]$; black pentagon - $[^1\text{C}_3^3\text{C}_3\text{im}][\text{NTf}_2]$; 13 ★ - $[^1\text{C}_2^3\text{C}_1\text{im}][\text{NTf}_2]$; ○ - $[^1\text{C}_3^3\text{C}_1\text{im}][\text{NTf}_2]$; * - $[^1\text{C}_4^3\text{C}_1\text{im}][\text{NTf}_2]$; △ - $[^1\text{C}_5^3\text{C}_1\text{im}][\text{NTf}_2]$.⁶¹ The dashed line highlights the $[^1\text{C}_{N-1}^3\text{C}_1\text{im}][\text{NTf}_2]$ series, which has no physical meaning.

and QOPNA, University of Aveiro, through the projects UID/CTM/50011/2013 and PEst-C/UI0062/2013; FCOMP-01-0124-FEDER-037296, respectively, financed by national funds through the FCT/MEC and when applicable cofinanced by FEDER under the PT2020 Partnership Agreement, and COST Action CM1206 - EXIL - Exchange on Ionic Liquids. The authors also thank FCT for the PhD and postdoctoral grants SFRH/BD/81261/2011, SFRH/BD/60513/2009, SFRH/BD/88369/2012 and SFRH/BD/70641/2010 from A.S.M.C. Rodrigues, M.A.A. Rocha, H.F.D. Almeida and C.M.S.S.N., respectively. M. G. Freire acknowledges the European Research Council (ERC) for the Starting Grant ERC-2013-StG-337753.

REFERENCES

- (1) Urahata, S. M.; Ribeiro, M. C. C. Structure of Ionic Liquids of 1-Alkyl-3-Methylimidazolium Cations: A Systematic Computer Simulation Study. *J. Chem. Phys.* **2004**, *120*, 1855–1863.
- (2) Wang, Y.; Voth, G. A. Unique Spatial Heterogeneity in Ionic Liquids. *J. Am. Chem. Soc.* **2005**, *127*, 12192–12193.
- (3) Canongia Lopes, J. N. A.; Pádua, A. A. H. Nanostructural Organization in Ionic Liquids. *J. Phys. Chem. B* **2006**, *110*, 3330–3335.
- (4) Bhargava, B. L.; Devane, R.; Klein, M. L.; Balasubramanian, S. Nanoscale Organization in Room Temperature Ionic Liquids: A Coarse Grained Molecular Dynamics Simulation Study. *Soft Matter* **2007**, *3*, 1395–1400.
- (5) Triolo, A.; Russina, O.; Bleif, H.-J.; Di Cola, E. Nanoscale Segregation in Room Temperature Ionic Liquids. *J. Phys. Chem. B* **2007**, *111*, 4641–4644.
- (6) Zheng, W.; Mohammed, A.; Hines, L. G.; Xiao, D.; Martinez, O. J.; Bartsch, R. A.; Simon, S. L.; Russina, O.; Triolo, A.; Quitevis, E. L. Effect of Cation Symmetry on the Morphology and Physicochemical Properties of Imidazolium Ionic Liquids. *J. Phys. Chem. B* **2011**, *115*, 6572–6584.
- (7) Rocha, M. A. A.; Lima, C. F. R. A. C.; Gomes, L. R.; Schröder, B.; Coutinho, J. A. P.; Marrucho, I. M.; Esperança, J. M. S. S.; Rebelo, L. P. N.; Shimizu, K.; Lopes, J. N. C.; et al. High-Accuracy Vapor Pressure Data of the Extended [C(n)C1im][Ntf2] Ionic Liquid Series: Trend Changes and Structural Shifts. *J. Phys. Chem. B* **2011**, *115*, 10919–10926.
- (8) Bernardes, C. E. S.; Shimizu, K.; Lobo Ferreira, A. I. M. C.; Santos, L. M. N. B. F.; Canongia Lopes, J. N. Structure and Aggregation in the 1,3-Dialkyl-Imidazolium Bis-(trifluoromethylsulfonyl)imide Ionic Liquid Family: 2. From Single to Double Long Alkyl Side Chains. *J. Phys. Chem. B* **2014**, *118*, 6885–6895.
- (9) Shimizu, K.; Bernardes, C. E. S.; Canongia Lopes, J. N. Structure and Aggregation in the 1-Alkyl-3-Methylimidazolium Bis-(trifluoromethylsulfonyl)imide Ionic Liquid Homologous Series. *J. Phys. Chem. B* **2014**, *118*, 567–576.
- (10) Martins, M. A. R.; Neves, C. M. S. S.; Kurnia, K. A.; Santos, L. M. N. B. F.; Freire, M. G.; Pinho, S. P.; Coutinho, J. A. P. Analysis of the Isomerism Effect on the Mutual Solubilities of Bis-(trifluoromethylsulfonyl)imide-Based Ionic Liquids with Water. *Fluid Phase Equilib.* **2014**, *381*, 28–35.
- (11) Rocha, M. A. A.; Coutinho, J. A. P.; Santos, L. M. N. B. F. Vapor Pressures of 1,3-Dialkylimidazolium Bis(trifluoromethylsulfonyl)imide Ionic Liquids with Long Alkyl Chains. *J. Chem. Phys.* **2014**, *141*, 134502–134508.
- (12) Kurnia, K. A.; Sintra, T. E.; Neves, C. M. S. S.; Shimizu, K.; Canongia Lopes, J. N.; Gonçalves, F.; Ventura, S. P. M.; Freire, M. G.; Santos, L. M. N. B. F.; Coutinho, J. A. P. The Effect of the Cation Alkyl Chain Branching on Mutual Solubilities with Water and Toxicities. *Phys. Chem. Chem. Phys.* **2014**, *16*, 19952–19963.
- (13) Almeida, H. F. D.; Freire, M. G.; Fernandes, A. M.; Lopes-da-Silva, J. A.; Santos, L. M. N. B. F.; Coutinho, J. A. P.; Morgado, P.; Shimizu, K.; Filipe, E. J. M.; Lopes, J. N. C.; et al. Cation Alkyl Side Chain Length and Symmetry Effects on the Surface Tension of Ionic Liquids. *Langmuir* **2014**, *30*, 6408–6418.
- (14) Rocha, M. A. A.; Ribeiro, F. M. S.; Schröder, B.; Coutinho, J. A. P.; Santos, L. M. N. B. F. Volatility Study of [C₁C₁im][NTf₂] and [C₂C₁im][NTf₂] Ionic Liquids. *J. Chem. Thermodyn.* **2014**, *68*, 317–321.
- (15) Rocha, M. A. A.; Neves, C. M. S. S.; Freire, M. G.; Russina, O.; Triolo, A.; Coutinho, J. A. P.; Santos, L. M. N. B. F. Alkylimidazolium Based Ionic Liquids: Impact of Cation Symmetry on Their Nanoscale Structural Organization. *J. Phys. Chem. B* **2013**, *117*, 10889–10897.
- (16) Bonhôte, P.; Dias, A.-P.; Papageorgiou, N.; Kalyanasundaram, K.; Grätzel, M. Hydrophobic, Highly Conductive Ambient-Temperature Molten Salts. *Inorg. Chem.* **1996**, *35*, 1168–1178.
- (17) Hunt, P. A. Why Does a Reduction in Hydrogen Bonding Lead to an Increase in Viscosity for the 1-Butyl-2,3-Dimethyl-Imidazolium-Based Ionic Liquids? *J. Phys. Chem. B* **2007**, *111*, 4844–4853.
- (18) Noack, K.; Schulz, P. S.; Paape, N.; Kiefer, J.; Wasserscheid, P.; Leipertz, A. The Role of the C2 Position in Interionic Interactions of Imidazolium Based Ionic Liquids: A Vibrational and NMR Spectroscopic Study. *Phys. Chem. Chem. Phys.* **2010**, *12*, 14153–14161.
- (19) Fumino, K.; Wulf, A.; Ludwig, R. Strong, Localized, and Directional Hydrogen Bonds Fluidize Ionic Liquids. *Angew. Chem., Int. Ed.* **2008**, *47*, 8731–8734.
- (20) Fumino, K.; Wulf, A.; Ludwig, R. The Cation-Anion Interaction in Ionic Liquids Probed by Far-Infrared Spectroscopy. *Angew. Chem., Int. Ed.* **2008**, *47*, 3830–3834.
- (21) Izgorodina, E. I.; Maganti, R.; Armel, V.; Dean, P. M.; Pringle, J. M.; Seddon, K. R.; MacFarlane, D. R. Understanding the Effect of the C2 Proton in Promoting Low Viscosities and High Conductivities in Imidazolium-Based Ionic Liquids: Part I. Weakly Coordinating Anions. *J. Phys. Chem. B* **2011**, *115*, 14688–14697.
- (22) Wieser, M. E.; Berglund, M. Atomic Weights of the Elements 2007 (IUPAC Technical Report). *Pure Appl. Chem.* **2009**, *81*, 2131–2156.
- (23) Sabbah, R. C.; Xu-wu, A.; Chickos, J. S.; Leitão, M. L. P.; Roux, M. V.; Torres, L. A. Reference Materials for Calorimetry and Differential Thermal Analysis. *Thermochim. Acta* **1999**, *331*, 93–204.
- (24) Roux, M. V.; Temprado, M.; Chickos, J. S.; Nagano, Y. Critically Evaluated Thermochemical Properties of Polycyclic Aromatic Hydrocarbons. *J. Phys. Chem. Ref. Data* **2008**, *37*, 1855–1996.
- (25) Paredes, X.; Fandiño, O.; Comuñas, M. J. P.; Pensado, A. S.; Fernández, J. Study of the Effects of Pressure on the Viscosity and Density of Diisodecyl Phthalate. *J. Chem. Thermodyn.* **2009**, *41*, 1007–1015.
- (26) Carvalho, P. J.; Regueira, T.; Santos, L. M. N. B. F.; Fernandez, J.; Coutinho, J. A. P. Effect of Water on the Viscosities and Densities of 1-Butyl-3-Methylimidazolium Dicyanamide and 1-Butyl-3-Methylimidazolium Tricyanomethane at Atmospheric Pressure. *J. Chem. Eng. Data* **2009**, *55*, 645–652.
- (27) Konicek, I. W. J.; Suurkuusk, J. A Precise Drop Heat Capacity Calorimeter for Small Samples. *Chem. Scr.* **1971**, *1*, 217–220.
- (28) Suurkuusk, J.; Wadsö, I. Design and Testing of an Improved Precise Drop Calorimeter for the Measurement of the Heat Capacity of Small Samples. *J. Chem. Thermodyn.* **1974**, *6*, 667–679.
- (29) Santos, L. M. N. B. F.; Rocha, M. A. A.; Rodrigues, A. S. M. C. M. C.; Štefja, V.; Fulem, M.; Bastos, M. Reassembling and Testing of a High-Precision Heat Capacity Drop Calorimeter. Heat Capacity of Some Polyphenyls at T=298.15K. *J. Chem. Thermodyn.* **2011**, *43*, 1818–1823.
- (30) Bernardes, C. E. S.; Santos, L. M. N. B. F.; Piedade, M. E. M.; da, A. New Calorimetric System to Measure Heat Capacities of Solids by the Drop Method. *Meas. Sci. Technol.* **2006**, *17*, 1405–1408.
- (31) Almeida, H. F. D.; Lopes-da-Silva, J. A.; Freire, M. G.; Coutinho, J. A. P. Surface Tension and Refractive Index of Pure and Water-Saturated Tetradecyltriethylphosphonium-Based Ionic Liquids. *J. Chem. Thermodyn.* **2013**, *57*, 372–379.
- (32) Almeida, H. F. D.; Passos, H.; Lopes-da-Silva, J. A.; Fernandes, A. M.; Freire, M. G.; Coutinho, J. A. P. Thermophysical Properties of

Five Acetate-Based Ionic Liquids. *J. Chem. Eng. Data* **2012**, *57*, 3005–3013.

(33) Almeida, H. F. D.; Teles, A. R. R.; Lopes-Da-Silva, J. A.; Freire, M. G.; Coutinho, J. A. P. Influence of the Anion on the Surface Tension of 1-Ethyl-3-Methylimidazolium-Based Ionic Liquids. *J. Chem. Thermodyn.* **2012**, *54*, 49–54.

(34) Tokuda, H.; Hayamizu, K.; Ishii, K.; Susan, M. A. B. H.; Watanabe, M. Physicochemical Properties and Structures of Room Temperature Ionic Liquids. 2. Variation of Alkyl Chain Length in Imidazolium Cation. *J. Phys. Chem. B* **2005**, *109*, 6103–6110.

(35) Domańska, U.; Rękawek, A.; Marciniak, A. Solubility of 1-Alkyl-3-Ethylimidazolium-Based Ionic Liquids in Water and 1-Octanol. *J. Chem. Eng. Data* **2008**, *53*, 1126–1132.

(36) Blokhin, A. V.; Paulechka, Y. U.; Strechan, A. A.; Kabo, G. J. Physicochemical Properties, Structure, and Conformations of 1-Butyl-3-Methylimidazolium Bis(trifluoromethanesulfonyl)imide [C4mim]-NTf₂ Ionic Liquid. *J. Phys. Chem. B* **2008**, *112*, 4357–4364.

(37) Ediger, M. D.; Angell, C. A.; Nagel, S. R. Supercooled Liquids and Glasses. *J. Phys. Chem.* **1996**, *100*, 13200–13212.

(38) Turnbull, D. Under What Conditions Can a Glass Be Formed? *Contemp. Phys.* **1969**, *10*, 473–488.

(39) Debenedetti, P. G.; Stillinger, F. H. Supercooled Liquids and the Glass Transition. *Nature* **2001**, *410*, 259–267.

(40) Nicholson, J. W. *The Chemistry of Polymers*; RSC Publishing, The Royal Society of Chemistry, 2006.

(41) Tariq, M.; Carvalho, P. J.; Coutinho, J. A. P.; Marrucho, I. M.; Lopes, J. N. C.; Rebelo, L. P. N. Viscosity of (C₂–C₁₄) 1-Alkyl-3-Methylimidazolium Bis(trifluoromethylsulfonyl)amide Ionic Liquids in an Extended Temperature Range. *Fluid Phase Equilib.* **2011**, *301*, 22–32.

(42) Gaciño, F. M.; Regueira, T.; Lugo, L.; Comuñas, M. J. P.; Fernández, J. Influence of Molecular Structure on Densities and Viscosities of Several Ionic Liquids. *J. Chem. Eng. Data* **2011**, *56*, 4984–4999.

(43) Wulf, A.; Fumino, K.; Ludwig, R. Spectroscopic Evidence for an Enhanced Anion-Cation Interaction from Hydrogen Bonding in Pure Imidazolium Ionic Liquids. *Angew. Chem., Int. Ed.* **2010**, *49*, 449–453.

(44) Rocha, M. A. A.; Bastos, M.; Coutinho, J. A. P.; Santos, L. M. N. B. F. Heat Capacities at 298.15 K of the Extended [CnC₁im][Ntf₂] Ionic Liquid Series. *J. Chem. Thermodyn.* **2012**, *53*, 140–143.

(45) Rocha, M. A. A.; Coutinho, J. A. P.; Santos, L. M. N. B. F. Evidence of Nanostructuring from the Heat Capacities of the 1,3-Dialkylimidazolium Bis(trifluoromethylsulfonyl)imide Ionic Liquid Series. *J. Chem. Phys.* **2013**, *139*, 104502–104507.

(46) Seki, S.; Tsuzuki, S.; Hayamizu, K.; Umebayashi, Y.; Serizawa, N.; Takei, K.; Miyashiro, H. Comprehensive Refractive Index Property for Room-Temperature Ionic Liquids. *J. Chem. Eng. Data* **2012**, *57*, 2211–2216.

(47) Miran Beigi, A. A.; Abdouss, M.; Yousefi, M.; Pourmortazavi, S. M.; Vahid, A. Investigation on Physical and Electrochemical Properties of Three Imidazolium Based Ionic Liquids (1-Hexyl-3-Methylimidazolium Tetrafluoroborate, 1-Ethyl-3-Methylimidazolium Bis(trifluoromethylsulfonyl) Imide and 1-Butyl-3-Methylimidazolium Methylsulfate). *J. Mol. Liq.* **2013**, *177*, 361–368.

(48) Tariq, M.; Forte, P. A. S.; Gomes, M. F. C.; Lopes, J. N. C.; Rebelo, L. P. N. Densities and Refractive Indices of Imidazolium- and Phosphonium-Based Ionic Liquids: Effect of Temperature, Alkyl Chain Length, and Anion. *J. Chem. Thermodyn.* **2009**, *41*, 790–798.

(49) Seoane, R. G.; Corderí, S.; Gómez, E.; Calvar, N.; González, E. J.; Macedo, E. A.; Domínguez, A.; Domínguez, Á. Temperature Dependence and Structural Influence on the Thermophysical Properties of Eleven Commercial Ionic Liquids. *Ind. Eng. Chem. Res.* **2012**, *51*, 2492–2504.

(50) Seoane, R. G.; González, E. J.; González, B. 1-Alkyl-3-Methylimidazolium Bis(trifluoromethylsulfonyl)imide Ionic Liquids as Solvents in the Separation of Azeotropic Mixtures. *J. Chem. Thermodyn.* **2012**, *53*, 152–157.

(51) Corderí, S.; González, B. Ethanol Extraction from Its Azeotropic Mixture with Hexane Employing Different Ionic Liquids as Solvents. *J. Chem. Thermodyn.* **2012**, *55*, 138–143.

(52) Lago, S.; Rodríguez, H.; Soto, A.; Arce, A. Deterpenation of Citrus Essential Oil by Liquid–Liquid Extraction with 1-Alkyl-3-Methylimidazolium Bis(trifluoromethylsulfonyl)amide Ionic Liquids. *J. Chem. Eng. Data* **2011**, *56*, 1273–1281.

(53) Gómez, E.; Calvar, N.; Macedo, E. A.; Domínguez, Á. Effect of the Temperature on the Physical Properties of Pure 1-Propyl 3-Methylimidazolium Bis(trifluoromethylsulfonyl)imide and Characterization of Its Binary Mixtures with Alcohols. *J. Chem. Thermodyn.* **2012**, *45*, 9–15.

(54) Andreatta, A. E.; Arce, A.; Rodil, E.; Soto, A. Physico-Chemical Properties of Binary and Ternary Mixtures of Ethyl Acetate + Ethanol + 1-Butyl-3-Methyl-Imidazolium Bis(trifluoromethylsulfonyl)imide at 298.15 K and Atmospheric Pressure. *J. Solution Chem.* **2010**, *39*, 371–383.

(55) Andreatta, A. E.; Francisco, M.; Rodil, E.; Soto, A.; Arce, A. Isobaric vapour–liquid equilibria and physical properties for isopropyl acetate + isopropanol + 1-butyl-3-methyl-imidazolium bis(trifluoromethylsulfonyl)imide mixtures. *Fluid Phase Equilib.* **2011**, *300*, 162–171.

(56) Jin, H.; O'Hare, B.; Dong, J.; Arzhantsev, S.; Baker, G. A.; Wishart, J. F.; Benesi, A. J.; Maroncelli, M. Physical Properties of Ionic Liquids Consisting of the 1-Butyl-3-Methylimidazolium Cation with Various Anions and the Bis(trifluoromethylsulfonyl)imide Anion with Various Cations. *J. Phys. Chem. B* **2008**, *112*, 81–92.

(57) Deetlefs, M.; Seddon, K. R.; Shara, M. Predicting Physical Properties of Ionic Liquids. *Phys. Chem. Chem. Phys.* **2006**, *8*, 642–649.

(58) Seki, S.; Tsuzuki, S.; Hayamizu, K.; Umebayashi, Y.; Serizawa, N.; Takei, K.; Miyashiro, H. Comprehensive Refractive Index Property for Room-Temperature Ionic Liquids. *J. Chem. Eng. Data* **2012**, *57*, 2211–2216.

(59) Adamson, A. W.; Gast, A. P. *Physical Chemistry of Surfaces*; John Wiley: New York, 1997.

(60) Miller, J. C.; Miller, J. N. *Statistical for Analytical Chemistry*; Hall, PTR Prentice: Chichester, NY, 1993.

(61) Carvalho, P. J.; Freire, M. G.; Marrucho, I. M.; Queimada, A. J.; Coutinho, J. A. P. Surface Tensions for the 1-Alkyl-3-Methylimidazolium Bis(trifluoromethylsulfonyl)imide Ionic Liquids. *J. Chem. Eng. Data* **2008**, *53*, 1346–1350.